

## Fermi surface nesting in $\text{Ba}_{1-x}\text{K}_x\text{BiO}_3$ observed by Compton scattering: Three-dimensional momentum density reconstruction study

N. Hiraoka,<sup>1,\*</sup> T. Buslaps,<sup>2</sup> V. Honkimäki,<sup>2</sup> J. Ahmad,<sup>3,†</sup> and H. Uwe<sup>3</sup>

<sup>1</sup>National Synchrotron Radiation Research Center, Hsinchu, 30076, Taiwan

<sup>2</sup>European Synchrotron Radiation Facility (ESRF), Boîte Postale 220, 38043 Grenoble Cedex 9, France

<sup>3</sup>Institute of Materials Science, University of Tsukuba, Tsukuba, Ibaraki 305-8573, Japan

(Received 22 January 2007; published 9 March 2007)

We have measured three-dimensional momentum densities in  $\text{Ba}_{1-x}\text{K}_x\text{BiO}_3$  using Compton scattering, where  $x=0.10$  (insulating) and  $0.37$  (metallic). The momentum densities reconstructed from experimental Compton profiles exhibit significant differences between the metallic and insulating samples. The momentum densities in the  $x=0.10$  insulating sample are interpreted to represent the filled, polyhedral Brillouin zone for fcc-type crystals, displaying a feature of the perfectly nested Fermi surface. The momentum densities in the  $x=0.37$  metallic sample resemble those predicted by band theory based on the local-density approximation, but still show an unusual feature due to Fermi-surface nesting. Those features, which showed some signatures in the two-dimensionally reconstructed data that we have previously reported, have been direct and compelling in the three-dimensionally reconstructed data in this study.

DOI: [10.1103/PhysRevB.75.121101](https://doi.org/10.1103/PhysRevB.75.121101)

PACS number(s): 71.18.+y, 71.45.Lr, 74.70.-b, 78.70.Ck

An energy spectrum of Compton-scattered x rays provides the electron momentum-density distribution  $[n(\mathbf{p})]$ , projected onto the scattering vector, i.e., the Compton profile (CP),  $J(p_z)$ .

$$J(p_z) = \int \int n(\mathbf{p}) dp_x dp_y, \quad (1)$$

where  $p_z$  is the momentum component along the scattering vector.<sup>1</sup> Each CP only provides one-dimensional (1D) information. However, the original 3D (or quasi-2D) momentum densities can be reconstructed from several CPs measured along different crystallographic orientations. With the  $n(\mathbf{p})$  reconstructed in the extended  $p$  space, one can obtain the occupation density in reduced  $k$  space,  $N_k$ , and finally determine the Fermi surface (FS), which is defined as the boundary between occupied and unoccupied states. An advantage of Compton scattering is that its application is not limited by the quality of the sample or its surface, unlike other techniques for FS studies.

Transport properties of solids are closely associated with the FS geometry. Therefore, Compton scattering, in principle, should reveal signatures of anomalies in conduction properties, such as the metal-insulator transition, the superconducting transition, or the occurrence of a charge-density wave (CDW). Nevertheless, there are few reports that have observed a clear evolution of momentum densities across such a transition using Compton scattering. The main reason is that only a few electrons near the FS are responsible for those transitions and it is difficult for Compton scattering, observing all the electrons in a sample, to detect such a small difference. A successful example is our previous study, reporting on the evolution of the momentum density in  $\text{Ba}_{1-x}\text{K}_x\text{BiO}_3$  across the metal to insulator transitions.<sup>2</sup>

The pseudocubic perovskites,  $\text{Ba}_{1-x}\text{K}_x\text{BiO}_3$ , exhibit complex electronic properties depending on the potassium concentration.<sup>3</sup> At  $x=0$ , the sample is an insulator having a monoclinic structure with ordered distortions of the

breathing-mode type.<sup>4</sup> The orthorhombic structure, having disordered distortions, appears at  $x \sim 0.10$ .<sup>5</sup> Furthermore, at  $x \sim 0.30$  the crystal transforms into a simple cubic (or tetragonal<sup>6</sup>) structure, accompanied by an insulator-to-metal transition. The metallic sample exhibits superconductivity at a critical temperature as high as 31 K between  $x=0.30$  and  $x=0.40$ .<sup>7</sup> At  $x \leq 0.3$ , major parts of the FS match the nesting condition, so that a stable insulating phase appears with a Peierls gap of  $1 \sim 2$  eV.<sup>8</sup> (The Peierls gap is a direct gap while the minimum gap is given by an indirect gap of  $\leq 1$  eV.) It is reported that this insulating phase is stabilized by (bi)polarons.<sup>9-11</sup>

In the previous report, we obtained 2D momentum densities, which were projected onto the (001) plane, for the  $x=0.13$  and  $x=0.39$  samples.<sup>2</sup> The 2D momentum densities exhibited evidence for the evolution of the FS. However, some important information of the FSs, being 3D in the real samples, was lost in the projection, which made intuitive understanding difficult. In the present study, we have observed a rigorous FS evolution by applying a 3D reconstruction method to new experimental data. Note that angle-resolved photoemission spectroscopy, which is one of the most sophisticated techniques for FS studies at present, is applicable to the 3D mapping of the FS (e.g., Ref. 12) but the actual applications are very rare because it is experimentally very demanding. It is also noted that positron annihilation experiment, sometimes used to determine 3D-FSs (e.g., Refs. 13 and 14), is not very suitable for this kind of sample. That is because the small distortion of the lattices can produce many domains, which trap positrons at their boundaries. This domain effect is also problematic for the de Haas van Alphen experiment, which requires high-quality samples to detect FS signals. Our present study demonstrates that it is possible to investigate the evolution of momentum densities or FSs using Compton scattering across the metal-insulator transitions or the occurrence of CDW in 3D systems as well as 1D or 2D ones.

The  $x=0.10$  and  $x=0.37$  single crystals, having a size of

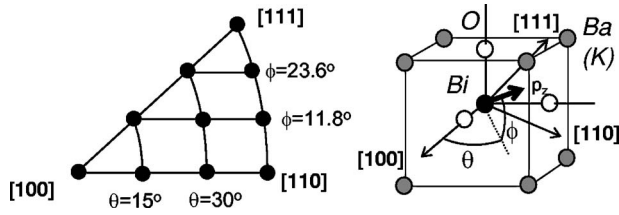


FIG. 1. Stereograph displaying the axes where CPs were measured ( $P_z$ ).

approximately  $5 \text{ mm}(\text{vertical}) \times 3 \text{ mm}(\text{horizontal}) \times 1 \text{ mm}$  (thick), were prepared by an electrochemical method.<sup>15,16</sup> For both crystals the [100] axis (in the cubic notation) was normal to the surface. The Compton-scattering experiments were carried out with the Laue-type dispersion-compensating spectrometer at ID15B, ESRF (France).<sup>17</sup> The incident photon energy was 88 keV, i.e., just below the K edge of Bi. These high-energy x rays have a penetration depth larger than  $100 \mu\text{m}$ , probing real bulk properties. The resolution varied between 0.12 and 0.18 atomic units (a.u.:  $1 \text{ a.u.} = 1.99 \times 10^{-24} \text{ kg m s}^{-1} = 1.89 \text{ \AA}^{-1}$ ), depending on the sample orientation. Ten CPs were measured along different directions in the irreducible wedge of the cubic Brillouin zone (BZ) for both the  $x=0.10$  and  $x=0.37$  samples (see Fig. 1), and around 100 000 counts were accumulated in the peak data channel (of bin size 0.02 a.u.) for each CP for half a day. The experiments were carried out at room temperature.

The code developed by Fajardo *et al.* was used to correct for multiple scattering,<sup>18</sup> while the reconstructions were made by the code of Tanaka *et al.*<sup>19</sup> The occupation densities (in  $k$  space) were obtained by folding the reconstructed momentum densities into the first cubic BZ based on the Lock-Crisp-West method.<sup>20</sup> It is shown in our previous report how those procedures transform the data on similar samples. In order to evaluate the propagation of statistical errors originating from the experimental data, we added artificial errors on theoretical CPs using random numbers, corresponding to the experimental statistical accuracies, and then carried out the reconstruction. The difference between the reconstructed momentum densities with and without errors provided the error propagation.<sup>21</sup>

The full-potential linearized augmented plane-wave (FLAPW) calculations based on the LDA band theory were carried out for comparisons with the experimental data.<sup>23</sup> For the  $x=0.37$  metallic phase, pseudoatoms having an atomic number ( $Z$ ) of 55.63 were placed at the Ba sites. The calculated band structure and the FS topology agreed well with those obtained by the Korringa-Kohn-Rostoker coherent potential approximation method used by Ref. 22. On the other hand, from our previous study we already know that the experimentally observed momentum densities in the insulating phase are well explained by the filled, polyhedral BZ due to the perfect nesting of the FS. The momentum densities in the insulating phase were calculated in the cubic  $2 \times 2 \times 2$  superlattice at  $x=0.0$ . A displacement of oxygen in the breathing-mode type ( $0.13 \text{ \AA}$ ) slightly larger than the real one ( $0.09 \text{ \AA}$ ) was necessary to stabilize the insulating phase without tilts of the  $\text{BiO}_6$  octahedron.

Figure 2 shows the occupation densities ( $N_k$ s), obtained

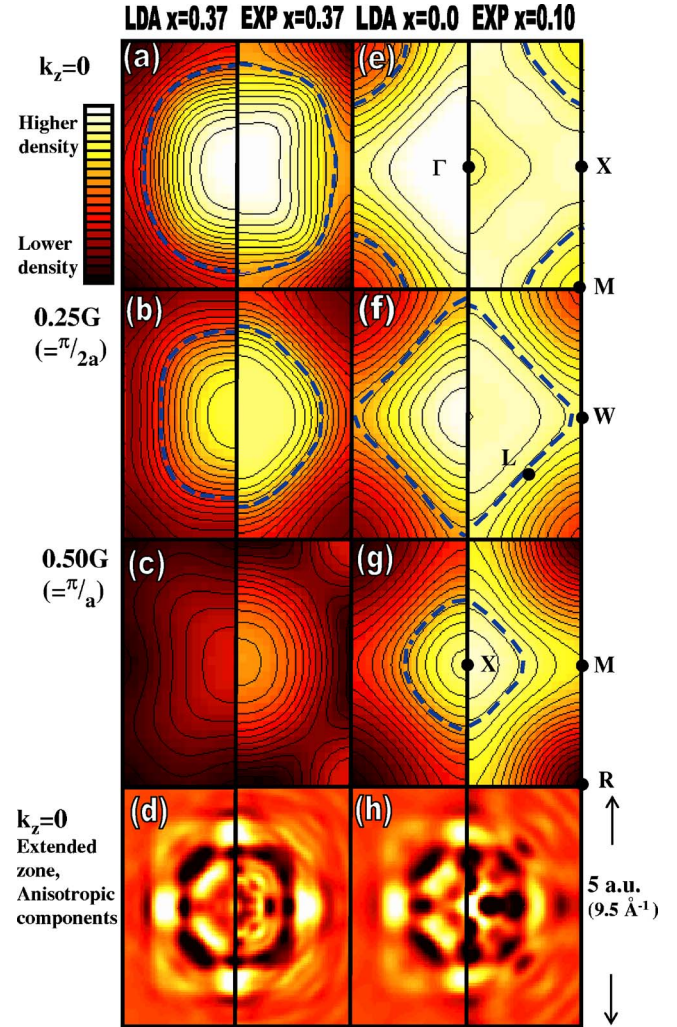


FIG. 2. (Color online) Slices of the occupation densities for  $x=0.37$  [(a), (b), and (c)] and for  $x=0.10$  (0.0) [(e), (f), and (g)]. Broken lines in each panel show the boundaries between occupied and unoccupied states, determined from the electron filling,  $1-x$ . They correspond to the FS and the BZ boundary in the metallic and the insulating samples, respectively. (d) and (h) are the momentum densities on the (001) planes in extended zones (before folding), where isotropic components are subtracted.

from the reconstruction method and the LCW folding, in the cubic BZ. Slices at  $k_z=0, 0.5\pi/a, \pi/a$  are shown for the  $x=0.37$  and  $x=0.10$  samples, where  $a$  is the lattice parameter. The right side of each panel shows experimental  $N_k$  while the left side shows the LDA theoretical  $N_k$ . For precise comparisons, the theoretical momentum densities were first converted to directional CPs, which were then reconstructed and folded in a similar approach to the experimental data. Here, the broadening effect due to the experimental resolution is included in the Fourier filtering functions during the reconstruction. It is generally a delicate procedure to determine the FS from momentum densities. Since the FS is defined as a discontinuous surface of the  $N_k$ , the derivative of the  $N_k$  can in principle be used to determine the FS. (For insulators, the derivatives should provide the surface corresponding to BZ boundaries.) However, it is pointed out that the derivative

does not always provide the correct FS, unless the momentum resolution is very high compared with the size of the FS or BZ.<sup>19</sup> In fact, we found an unrealistically large FS for the  $x=0.37$  sample when we employed this approach. Since the experimental resolution achievable was about 0.1 a.u. (13% of the BZ), we have determined the FS by applying the following procedure. We calculated the volume inside various isodensity surfaces of the occupation densities, and determined the FS or the boundary between occupied and unoccupied states as the isodensity surface in which the volume coincided with the number of conduction electrons, i.e., 0.63 ( $x=0.37$ ) or 0.9 ( $x=0.10$ ). This analysis is based on Luttinger's theorem, which states that the volume inside the FS is invariant even for correlated electrons. When we applied this procedure to the density reconstructed from *theoretical* CPs for  $x=0.37$ , the obtained FS agreed with the original FS within an accuracy of a few percent. Even though this is not an exact procedure, such accuracy is sufficient to observe the main features of the FS nesting, which is the central issue in this study. The determined boundaries between occupied and unoccupied states are shown with the broken lines in the contour maps of Fig. 2.

Figure 3 shows the 3D representations of the boundary surfaces between occupied and unoccupied states. The evolution of the FS is clearly seen across the metal-insulator transition. The FS nesting in the  $x=0.10$  insulating sample is directly visible. The  $x=0.10$  data exhibit a similar topology as the BZ for fcc crystals resulting from perfect nesting. Here, we have used an electron filling of 0.9 to determine the boundary surface from the  $x=0.10$  experimental data [Fig. 3(c)]. Its geometry appears even more similar to Fig. 3(d) if the filling of 1.0 is assumed (not shown).

Even though the LDA apparently fails to reproduce the insulating phase for  $x=0.10$ , it may nevertheless be interesting to consider its predicted FS. This complements the comparison between the experimental data for  $x=0.10$  [Fig. 3(c)] and the LDA result for  $x=0.0$  [Fig. 3(d)]. Figures 3(e) and 3(f) show the  $x=0.10$  LDA-FS, where the holes are doped by pseudoatoms having  $Z=55.9$ . The LDA predicts the appearance of hole pockets around the X points in the BZ [see Fig. 3(e)]. These hole pockets are not well resolved after the reconstruction (because of the Fourier filtering that introduces a broadening comparable with the experimental resolution), but they manifest themselves as significantly reduced necks [Fig. 3(f)]. The fact that the  $x=0.10$  experimental data are explained well by the LDA for  $x=0.0$ , rather than that for  $x=0.10$ , reconfirms the disappearance of the hole pocket with decreasing potassium concentration.

In fact, a nesting feature is also discernible in the experimental data for the  $x=0.37$  metallic sample [Fig. 3(a)]. The FS touches the (111) zone boundary planes, showing a weak nesting feature at the L points. Therefore, the cubiclike FS that is predicted by the LDA is not seen in the experimental FS. In our previous report, the 2D occupation density projected onto the (001) plane exhibited an unusual feature at  $(0.5\pi/a, 0.5\pi/a)$ . The present data show direct evidence of the nesting feature at the L points  $(0.5\pi/a, 0.5\pi/a, 0.5\pi/a)$  in the BZ.

One of the central issues in the insulating phase is the behavior of the doped holes. A reasonable prediction for this

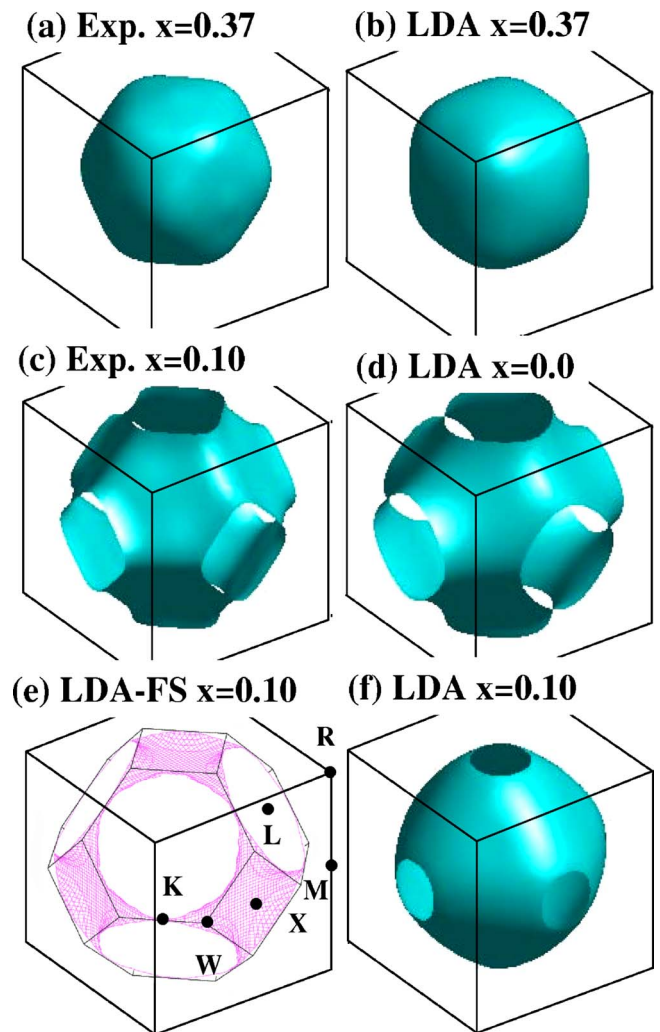


FIG. 3. (Color online) 3D representations of the boundary surfaces between occupied and unoccupied states, determined from the electron filling,  $1-x$ . The LDA provides an insulating phase for the  $x=0.0$  superlattice (d), so that the boundary surface corresponds to the BZ for fcc crystals [solid lines in (e)].

is provided by the (bi)polaron model of Bischofs *et al.*<sup>9</sup> In this model, the doped holes become localized (bi)polarons because the movement of the holes changes the valence number of the Bi atoms, leading to the expansion (contraction) of the  $\text{BiO}_6$  octahedron; this model is compatible with our data. The boundary surface between occupied and unoccupied states in the  $x=0.10$  experimental data resembles that of the  $x=0.0$  LDA as if the doped holes had disappeared, as already discussed. Localized charges, such as heavy polarons, can escape from the detection of Compton scattering because they have a broad distribution in momentum space.<sup>24</sup>

Another prominent difference between theory and experiment is the high occupation density around the M points in the  $x=0.10$  experimental data [Fig. 2(e)], which arises from the low contrast of the occupation densities in the (001) plane. This is not very surprising. It is well known that electron correlation can transfer some electrons from inside a FS (the first BZ for fcc crystals, in this case) to the outside. In

addition to this, the Ba/K disorder effect, which is not taken into account in our calculation, might also be significant. Since Ba and K significantly differ in charge and mass, the lattice periodicity could be strongly disturbed.<sup>6</sup>

In summary, we have measured the electron momentum distributions in  $\text{Ba}_{1-x}\text{K}_x\text{BiO}_3$ , where  $x=0.10$  (insulating) and  $x=0.37$  (metallic), using Compton scattering. The 3D momentum densities reconstructed from the Compton profiles exhibited a significant evolution across the insulator-metal transitions. The boundary surface between occupied and unoccupied states, determined in the  $x=0.10$  experimental data, agreed well with the topology of the Brillouin zone for fcc crystals as the LDA band theory provided for  $x=0.0$ . This represents the feature of a perfectly nested Fermi surface,

suggesting the disappearance of the hole pockets that are predicted by the theory to be around the  $X$  points in the Brillouin zone. The experimentally determined Fermi surface for the  $x=0.37$  sample resembled that of the LDA band theory. However, a weak nesting feature of the Fermi surface was observed near the  $L$  points. Although these conclusions are basically the same as those of our previous report, in this study they have been directly visible and compelling.

We would like to thank Y. Tanaka for providing us with the reconstruction program. We are also grateful to Y. Q. Cai for supporting this study. For the calculations of the LDA Fermi surfaces, the BANDS01 code of the beamline BL08W, SPring-8 was used.

\*Electronic address: hiraoka@spring8.or.jp

<sup>†</sup>Present address: Department of Physics, Bahauddin Zakariya University, Multan 60800, Pakistan.

- <sup>1</sup>P. Eisenberger and P. M. Platzman, *Phys. Rev. A* **2**, 415 (1970).
- <sup>2</sup>N. Hiraoka, T. Buslaps, V. Honkimäki, H. Minami, and H. Uwe, *Phys. Rev. B* **71**, 205106 (2005).
- <sup>3</sup>S. Pei, J. D. Jorgensen, B. Dabrowski, D. G. Hinks, D. R. Richards, A. W. Mitchell, J. M. Newsam, S. K. Sinha, D. Vaknin, and A. J. Jacobson, *Phys. Rev. B* **41**, 4126 (1990).
- <sup>4</sup>D. E. Cox and A. W. Sleight, *Solid State Commun.* **19**, 969 (1976).
- <sup>5</sup>S. Salem-Sugui, Jr, E. E. Alp, S. M. Mini, M. Ramanathan, J. C. Campuzano, G. Jennings, M. Faiz, S. Pei, B. Dabrowski, Y. Zheng, D. R. Richards, and D. G. Hinks, *Phys. Rev. B* **43**, 5511 (1991).
- <sup>6</sup>M. Braden, W. Reichardt, E. Elkaim, J. P. Lauriat, S. Shiryayev, and S. N. Barilo, *Phys. Rev. B* **62**, 6708 (2000).
- <sup>7</sup>D. G. Hinks, B. Dabrowski, J. D. Jorgensen, A. W. Mitchell, D. R. Richards, S. Pei, and D. Shi, *Nature (London)* **333**, 836 (1988).
- <sup>8</sup>S. H. Blanton, R. T. Collins, K. H. Kelleher, L. D. Rotter, Z. Schlesinger, D. G. Hinks, and Y. Zheng, *Phys. Rev. B* **47**, 996 (1993).
- <sup>9</sup>I. B. Bischofs, V. N. Kostur, and P. B. Allen, *Phys. Rev. B* **65**, 115112 (2002).
- <sup>10</sup>T. Nishio, J. Ahmad, and H. Uwe, *Phys. Rev. Lett.* **95**, 176403 (2005).
- <sup>11</sup>J. Ahmad and H. Uwe, *Phys. Rev. B* **72**, 125103 (2005).
- <sup>12</sup>N. Kamakura, Y. Takata, T. Tokushima, Y. Harada, A. Chainani, K. Kobayashi, and S. Shin, *Phys. Rev. B* **74**, 045127 (2006).

- <sup>13</sup>S. B. Dugdale, H. M. Fretwell, M. A. Alam, G. Kontrym-Sznajd, R. N. West, and S. Badrzadeh, *Phys. Rev. Lett.* **79**, 941 (1997).
- <sup>14</sup>M. Biasini, G. Kontrym-Sznajd, M. A. Monge, M. Gemmi, A. Czopnik, and A. Jura, *Phys. Rev. Lett.* **86**, 4616 (2001).
- <sup>15</sup>H. Minami, T. Nishio, and H. Uwe, in *Advances in Superconductivity VIII*, Proceedings of the 8th ISS'95 Hamamatsu (Hamamatsu, 1996), p. 429.
- <sup>16</sup>T. Nishio, H. Minami, and H. Uwe, *Physica C* **357–360**, 376 (2001).
- <sup>17</sup>N. Hiraoka, T. Buslaps, V. Honkimäki, and P. Suortti, *J. Synchrotron Radiat.* **12**, 670 (2005).
- <sup>18</sup>P. Fajardo, V. Honkimäki, T. Buslaps, and P. Suortti, *Nucl. Instrum. Methods Phys. Res. B* **134**, 337 (1998).
- <sup>19</sup>Y. Tanaka, Y. Sakurai, A. T. Stewart, N. Shiotani, P. E. Mijnarends, S. Kaprzyk, and A. Bansil, *Phys. Rev. B* **63**, 045120 (2001).
- <sup>20</sup>D. G. Lock, V. H. C. Crisp, and R. N. West, *J. Phys. F: Met. Phys.* **3**, 561 (1973).
- <sup>21</sup>N. Hiraoka, T. Buslaps, V. Honkimäki, H. Guyot, and C. Schlenker, *Phys. Rev. B* **71**, 125417 (2005).
- <sup>22</sup>S. Sahrakorpi, B. Barbiellini, R. S. Markiewicz, S. Kaprzyk, M. Lindroos, and A. Bansil, *Phys. Rev. B* **61**, 7388 (2000).
- <sup>23</sup>A. Kodama, N. Hamada, and A. Yanase, Computer code BANDS01, Fuji Research Inst. Corp. See, e. g., M. Umekawa, N. Hamada, A. Kodama, and Y. Moritomo, *J. Phys. Soc. Jpn.* **73**, 430 (2004) for details of the calculation.
- <sup>24</sup>A shallow dip, discernible in the occupation densities of the  $x=0.10$  experimental data around  $\Gamma$ , could arise from (bi)polarons derived from doped holes, but this structure does not exceed our estimated error bars.